Materials Advances

ROYAL SOCIETY OF CHEMISTRY

PAPER

View Article Online
View Journal | View Issue



Cite this: *Mater. Adv.*, 2022, 3, 5488

# Chitosan entrapped microporous activated carbon composite as a supersorbent for remazol brilliant blue R

Pradip M. Nandanwar,[a] D. Saravanan,[b] Pankaj Bakshe[a] and Ravin M. Jugade *[a]

Received 5th May 2022,
Accepted 24th May 2022

DOI: 10.1039/d2ma00508e

rsc.li/materials-advances

In this work, we synthesized a chitosan-activated carbon composite (Cs–C) using sodium tripolyphosphate (STTP) as a crosslinker. The Cs–C was characterized through Fourier transform infrared, X-ray diffraction, scanning electron microscopy, energy dispersive X-ray spectroscopy, and the pH point of zero charge for the physicochemical, structural, and morphological analyses. The material was subjected to the adsorption of Remazol Brilliant Blue R (RBBR) dye. The effects of the solution pH, adsorbent dose, contact time, temperature, and dye concentration were examined. The equilibrium data was described well by the Langmuir isotherm model with a coefficient of determination ($R^2$) value of 0.9994 and chi-square value of 6.94. At near-neutral pH, with a contact time of only 60 min at room temperature, the material showed an extremely high adsorption capacity of 540.3 mg $g^{-1}$ which is much higher in contrast to all the previously reported materials. The kinetics of uptake was well-described by the pseudo-second-order model chemisorption model. Evaluation of the thermodynamic parameters reflected the spontaneous, endothermic and entropy-driven nature of the adsorption.



## Introduction

Being one of the essential aspect of all lives on earth, water defines the characteristic of human beings. With a very limited accessibility of pure water on earth, unfortunately the rapid increase in water pollution is posing a challenge due to industrial and anthropogenic contamination in water bodies.[1] The main toxicants include dyes,[2] pesticides,[3] colouring matter,[4] and oils.[5] Among the various concerns, textile industries are the major contributors towards the environmental pollution due to the discharge of various dyes in water bodies.[6] The dyeing industry waste is one of the major concerns of the textile industry, including coloured waste water, which causes hazardous effects on the environment. Majority of these dyes have a complex aromatic molecular structure, and are water soluble, non-biodegradable, and toxic in nature; therefore, it has become highly important to remove these dyes from water effluents to make the environment safe and clean in terms of protecting the livelihoods of all creatures.[7]

Reactive dyes are used for dyeing cellulosic fibres in textile industries to a large extent, and these are usually characterized by azo bonds. The colour of azo dyes is due to a chromophoric effect of the azo group. First, the dyes are treated with cellulose and then are made to interact with the fibrous material of the cellulose.[8] The reaction occurs by the formation of a covalent bond between the dye molecule and the fibre. Adsorption, electrochemical oxidation, biological treatment, coagulation, physicochemical flocculation, precipitation, ozonation, and other comprehensive technologies have been applied and critically reviewed recently.[9–13] Conventional wastewater treatment methods have a low removal efficiency.[14] The adsorption process was found to be one of the effective techniques among several chemical, bacteriological, catalytic, and physical methods that have been successfully employed for the removal of colours from waste water due to its low cost, ease of operation, greater efficiency, and non-generation of toxic materials.[15]

Several adsorbents have been tested for their applicability in dye adsorption from effluents, such as activated sludge,[16] alum,[17] coal ash,[18] silicates,[19] acetyl acetone,[20] and graphene-based nanomaterials.[21] The ability of chitosan to remove contaminants from effluents is highly appreciated due to its diverse functionality, including amino and hydroxyl functional groups in the molecule for forming various interactions, including hydrogen bonding, electrostatic interaction, and van der Waals forces of attraction.[22] However, the insufficient strength and stability in acidic medium hinder the greater application of chitosan.[23] In order to resolve these issues and to improve the physicochemical properties of chitosan, its modifications using various crosslinkers as well as by composite formation with mechanically and thermally stable materials are the most obvious

[a] *Department of Chemistry, RTM Nagpur University, Nagpur, 440033, India. E-mail: ravinj2001@yahoo.co.in*
[b] *National College, Tiruchirapalli, Tamilnadu, India*

pathways. Composites of chitosan with activated charcoal can be applied to improve the surface structure, morphology, and surface-assimilative property of chitosan biopolymers.[24] Adding a crosslinking agent enhances the chemical stability and leads to microstructure improvement for its improved adsorption performance.[25] Several studies have been carried out on the adsorption of water pollutants using chitosan-activated charcoal composites involving the removal of dyes in the recent years.[26–28]

Recently, we reported a composite of cellulose fabricated by the co-precipitation of Fe and Al in the cellulose material for the detoxification of various reactive dyes with high adsorption capacities.[29] In this study, we used a hybrid approach involving crosslinking chitosan with sodium tripolyphosphate (STTP) for imprioved mechanical strength and for entrapping activated carbon through the enhanced surface area and porosity, leading to a supersorbent with excellent confiscation capability for RBBR dye.

## Experimental

### Reagents

All the chemicals and reagents used in the experiments were of analytical grade. Chitosan with a degree of deacetylation of >90% was purchased from Sisco Research Laboratory, India. Acetic acid and 25% ammonia solution were obtained from SD Fine Chemicals Ltd (India). Activated charcoal, STTP, and Remazol brilliant blue R dye were acquired from Loba Chemie (India). All the chemicals were used without further purification and deionized distilled water was used throughout the studies.

### Instruments

FT-IR spectra were obtained using a Bruker AlphaE spectrometer (USA) for an average of 23 scans. A Rigaku Miniflex 300 system (Tokyo, Japan) was used for the XRD analysis. The surface morphology was studied by a scanning electron microscopy (SEM) system model TESCAN VEGA 3 SBH (Czech Republic), while EDX analysis was performed by an X-ray analyzer on an Oxford INCA Energy 250 EDS system during the SEM observations. Thermal analysis was carried out using a DTG-60 simultaneous DTA/TG instrument (Shimadzu, Japan) at a scan rate of 20 °C $min^{-1}$ and in a nitrogen flow rate of 100 mL $min^{-1}$. The Brunauer–Emmett–Teller surface area was estimated by the nitrogen adsorption–desorption method on a Quantachrome Nova 2200e analyzer (Florida). The estimation of dye concentration was carried out using an Equiptronics EQ-824 instrument (India) at the dye absorption maxima of 594 nm.

### Synthesis of the adsorbent

Chitosan solution was prepared using a previously reported method[30] by dissolving 5 g chitosan in 500 mL of 2% acetic acid. To dissolve chitosan in acetic acid, it was added gradually by keeping it under magnetic stirring for 60 min. After the complete dissolution of chitosan in acetic acid, 2.5 g activated charcoal was added step by step and the solution was kept on gentle stirring for 30 min. The resultant solution was dripped into a beaker containing 1000 mL of 6% ammonia solution with the help of a syringe, leading to the formation of spherical beads. The fresh beads were rinsed with distilled water several times for removal of all traces of ammonia. Next, 250 mL of 1% solution of STTP crosslinker was added to the beads and with very gentle stirring on a magnetic stirrer at 40 °C for 2 h. The resulting Cs–C beads were washed with distilled water several times and dried overnight in a hot air oven at 50 °C. The beads were crushed by a pestle and mortar and sieved to −100 micron mesh before being used in the adsorption experiments.

### Batch adsorption tests

In each experiment, 25 mL dye solution of a predecided concentration along with a known weight of Cs–C, was stirred on a magnetic stirrer for a predetermined time. It was then filtered and the residual concentration of the solution was evaluated spectrophotometrically. Triplicate observations were obtained and the mean values were reported. The equilibrium adsorption efficiency in mg $g^{-1}$ was calculated as-[31]

$$q_e = \frac{(C_0 - C_e)V}{W}$$

where Co (mg $L^{-1}$) and Ce (mg $L^{-1}$) are the dye concentration initially and at equilibrium, respectively, while W (g) is the weight of adsorbent used in the respective study.

Trial runs were performed to compare the adsorption efficiencies of unmodified and sequentially modified adsorbents for the RBBR dye. For this, 50 mg $L^{-1}$ dye solution was equilibrated for 60 min with 100 mg of unmodified chitosan, activated charcoal, STTP crosslinked chitosan, and Cs–C composite in different flasks. The solution phase concentrations in each flask were determined after filtration and the adsorption efficiency was calculated for each of them.

The $pH_{PZC}$ of Cs–C was determined by a previously reported method[32] in order to establish the surface charge on the adsorbent. For this, 50 mL 0.1 M NaCl solutions with varying initial pH from 2.0 to 9.0 were taken in a series of conical flasks. These solutions were stirred with 100 mg of Cs–C for 24 h. The final pH of the supernatant solutions were measured. A graph was plotted of the change in pH as a function of the initial pH, with the point it intersects the *x*-axis called the pH point of zero charge.

For studying the effect of the initial solution pH on the adsorption efficiency, a series of dye solutions of 100 mg $L^{-1}$ were prepared and their pH was varied from 4.0 to 9.0. To each of the systems, 100 mg of Cs–C adsorbent was administered and equilibrated for 30 min. After that, the systems were filtered and the absorbance values were obtained.

The kinetics of adsorption was studied by equilibrating 100 mg $L^{-1}$ dye solution with 25, 50, and 100 mg of Cs–C from 5 to 150 min. The residual solution phase dye concentration was determined after filtration.

In order to study the effect of the initial dye concentration, various dye concentrations from 20 to 400 mg $L^{-1}$ were equilibrated with 25, 50, and 100 mg Cs–C for 60 min and then the dye concentration in the solution was determined.

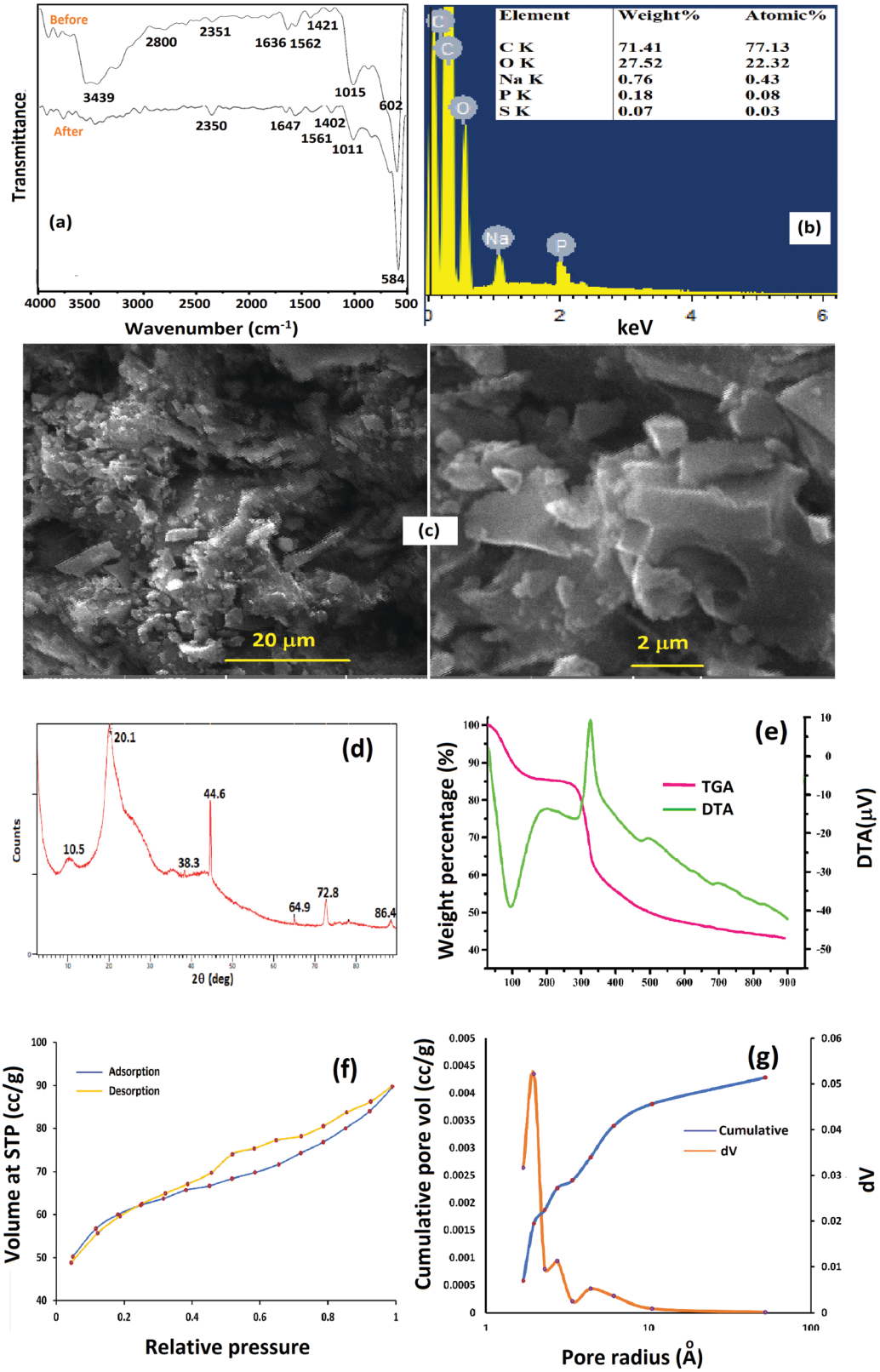


Fig. 1 (a) FT-IR spectra of Cs–C before and after the adsorption of RBBR. (b) EDX spectrum and elemental composition of Cs–C and (c) SEM micrographs of Cs–C at two different resolutions. (d) XRD spectrum, (e) TGA–DTA curve, (f) $N_2$ adsorption–desorption curves, and (g) pore-size distribution curves of Cs–C.

The Cs–C dose was increased from 25 to 300 mg. Four dye concentrations of 50, 100, 150, and 200 mg $L^{-1}$ were stirred with various doses of Cs–C for the optimized contact time of 60 min and then their final concentrations were determined spectrophotometrically.

To study the effect of temperature as part of the evaluation of the thermodynamics parameters, the temperature was varied from 298 to 333 K. The quantity of adsorption of RBBR upon Cs–C was investigated at an initial RBBR concentration of 100 mg $L^{-1}$ using a 25 mL volume and adsorbent dose of 100 mg.

## Results and discussion

### Characterization of Cs–C

Fig. 1a depicts the FT-IR spectra of Cs–C and Cs–C after RBBR dye adsorption. The Cs–C spectrum showed a characteristic broad peak around 3440 $cm^{-1}$ corresponding to the stretching vibrations of –NH and –OH bonds in chitosan along with a skeletal vibration peak of C–O–C at 1015 $cm^{-1}$.[33] A highly intense peak at 602 $cm^{-1}$ corresponding to O–P–O bending of the STTP group confirmed the crosslinking of chitosan with STTP. Peaks observed at 1630 and 1562 $cm^{-1}$ could be attributed to the linkage between the phosphoric and ammonium ions. These results were attributed to the crosslinking between the amino groups of chitosan and phosphate groups of STPP.[34] After adsorption of the dye on the Cs–C surface, the important peaks were found to shift from their positions, indicating an interaction between the adsorbate and adsorbent molecules. The reduction in the intensity of the peak around 3440 $cm^{-1}$ was an indication of the strong interaction between –OH and $-NH_2$ groups of chitosan with the RBBR molecules, consistent with the reported literature.[35]

The crosslinking could be further confirmed by EDX studies of Cs–C (Fig. 1b). The EDX spectrum showed the important peaks for phosphorous and sodium along with those of carbon and oxygen, indicating the incorporation of tripolyphosphate moieties in the chitosan framework.

The SEM micrographs of Cs–C (Fig. 1c) revealed that the surface was non-uniform and heterogenous. This heterogeneity led to an overall enhancement in the surface area and hence in the adsorption efficiency.

XRD analysis was carried out to determine the crystalline and/or amorphous nature of Cs–C, as shown in Fig. 1d.[36] The diffractogram clearly showed the characteristic peaks of chitosan at $2\theta$ = 10.5° and 20.1°, corresponding to the (020) and (110) planes. The slightly crystalline nature of the chitosan matrix could be attributed to the intermolecular and intramolecular hydrogen bonding. The XRD pattern of Cs–C showed additional peaks at $2\theta$ = 44.5° and 64.9°, which were typical for the tripolyphosphate crosslinked chitosan.[37,38]

The TGA curve of Cs–C. (Fig. 1e) showed a small weight loss of about 15% up to 150 °C associated with an endothermic crest in the DTA curve corresponding to the loss of moisture. A second major weight loss of about 50–55% occurred between 330 °C and 500 °C and was associated with an exothermic peak in the DTA curve indicating the degradation of the polymeric organic framework.[39]

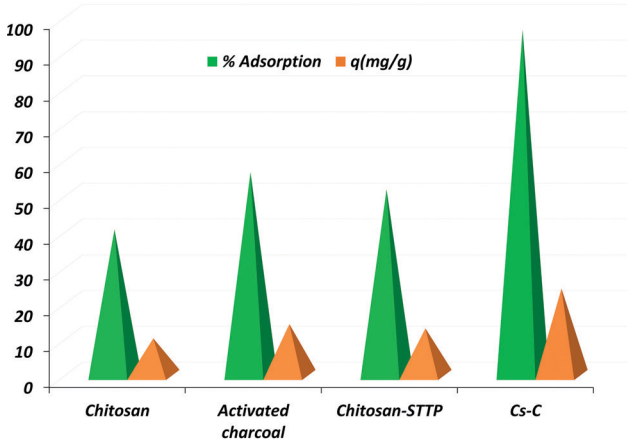


Fig. 2 Comparison of the adsorption efficiencies of various materials.

The pore dimensions and surface area of Cs–C were determined by $N_2$ adsorption–desorption isotherms, as depicted in Fig. 1f, while the pore-size distribution is shown in Fig. 1g. The surface area of the unmodified chitosan was found to be 0.65 $m^2\ g^{-1}$ which was found to be enhanced to 190 $m^2\ g^{-1}$ in the Cs–C composite. These values were obtained by BET isotherm. As Cs–C was a porous material, its pore properties were established through the BJH method using the nitrogen adsorption–desorption curve. The pore volume was found to be 1.388 $m^3\ g^{-1}$, showing the highly porous nature of the material in contrast to native chitosan, which is completely non-porous in nature. The mean pore radius of 1.459 nm was an indication of the microporous nature of the composite. As shown in Fig. 1f, the $N_2$ physisorption isotherm could be assigned as a type IV hysteresis on the basis of IUPAC classification. This indicated the presence of micropores in the Cs–C structure.[40]

Activated charcoal (AC) has a large surface area and microporous structure. The incorporation of AC in the chitosan matrix led to an enhancement of the adsorption of anionic RBBR dye molecules on the Cs–C surface because of the high diffusion of RBBR dye molecules through the micropores of Cs–C.[41] The hysteresis loop (Fig. 1g) was clear evidence of the presence of micro- and mesopores in the composite material. This observation was consistent with the flake-like appearance of the surface of the material as obtained in the SEM micrographs. The shift in the desorption curve towards the left was due to the cavitation-driven desertion.[42,43] The high adsorption capacity of the Cs–C composite towards RBBR could be prominently attributed to the high surface area, large pore volume, and micro- and mesoporous nature of the adsorbent.

### Batch adsorption studies

During the trial experiments with unmodified chitosan, pure activated charcoal, chitosan crosslinked with STTP, and the final composite Cs–C, each of the materials adsorbed RBBR dye to a different extent. It was observed that Cs–C adsorbed 96.4% of the dye with an adsorption efficiency of 24 mg $g^{-1}$ in just

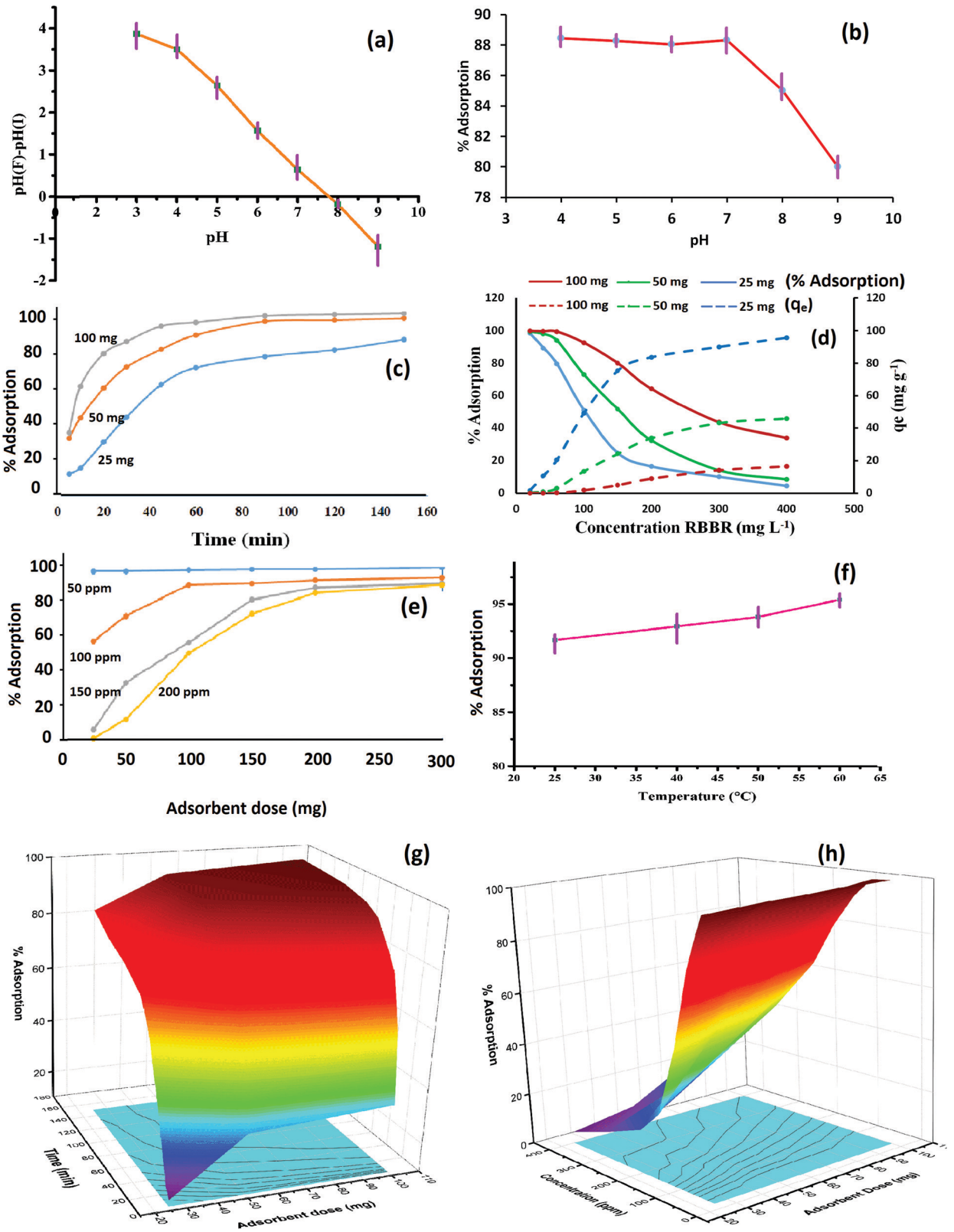


Fig. 3 (a) pHpzc of Cs–C. Effect of: (b) the solution pH, (c) contact time, (d) initial dye concentration, (e) adsorbent dose, and (f) temperature on the adsorption efficiency. (g) Dose-time dependence and (h) dose-concentration dependence.

60 min, and so it was established to be the best material compared to any of the precursors (Fig. 2). Both chitosan as well as activated charcoal had a tendency to adsorb RBBR dye to some extent. However, the combination of the two led to a much effective adsorption owing to the enhanced surface area of charcoal and the effective molecular interactions of chitosan. Similar results were reported by Khapre ***et al.*** (2020) for successively modified materials towards alizarin red S dye.

The effects of various variables in the adsorption experiments are presented in Fig. 3. The pH at which the surface charge on Cs–C was zero, *i.e.* the pHpzc was found to be 7.8, representing that the material exhibited a near-neutral pHpzc (Fig. 3a), meaning that the Cs–C surface would be distinctly positive below pH 7.8 and negative above pH 7.8. It was observed that there was no significant effect of pH on the removal efficiency of dye from pH 4 to 7 (Fig. 3b). In this pH range, the surface charge on Cs–C was positive, indicating a strong attractive interaction with the anionic dye molecules. In acidic pH, the $-NH_2$ group of chitosan was protonated as $-NH_3^+$ while the RBBR dye has an $-SO_3^-$ group, which would be responsible for the interaction in the acidic range.[44] Strong electrostatic forces between the adsorbent and adsorbate were responsible for the high adsorption capacity of Cs–C towards RBBR dye. However, with the increase in pH above 7.8, the adsorption efficiency was found to be reduced at pH 8 and 9. This was quite obvious and could be related to the surface charge of the adsorbent. Hence, the original solution with pH 6.0 was used in all the studies.

The increase in the adsorption duration from 5 min to 150 min showed a rapid increase in adsorption in the beginning. This could be attributed to the available surface for the adsorbent molecules in the beginning. As the surface got covered with the dye, the percentage adsorption reached almost saturation in 60 min. After 60 min, there was a negligible hike in removal efficiency, and so the contact time of 60 min was considered optimum for RBBR dye (Fig. 3c). This was quite obvious as the maximum number of sites were available on the Cs–C surface in the beginning, but over time the sites get occupied by dye molecules, and equilibrium is reached in about 60 min.[45]

The increase in RBBR concentration led to a reduction in the percentage adsorption but increase in the value of $q_e$ (Fig. 3d). As the concentration of incoming RBBR molecules increased, the relative availability of active adsorption sites decreased, thus lowering the removal percentage. However, the gathering of the excess dye on the adsorbent surface enhanced its adsorption capacity in terms of mg of dye adsorbed per gram of adsorbate material. As the adsorbent dose was increased, the availability of the surface increased and so the accumulation per unit mass ($q_e$) went on decreasing with the increase in adsorbent dose for the same concentration. With this context, an initial dye concentration of 100 mg $L^{-1}$ was fixed for the further studies.

As the Cs–C amount was increased from 25 mg to 300 mg, the availability of a greater number of active adsorption sites led to an enhancement in the adsorption percentage (Fig. 3e). For 100 mg $L^{-1}$ solution, an adsorbent dose of 100 mg was found to give more than 90% adsorption, and so this dose was selected as the optimum dose.

Table 1 RBBR dye adsorption on Cs–C in terms of the kinetics, isotherm, and thermodynamics parameters

| Studies | Model | Parameter | Observation |
|---|---|---|---|
| Kinetics studies | PFO | $K_1$ ($min^{-1}$) | 0.0456 |
| | | $q_e$ cal (mg $g^{-1}$) | 62.01 |
| | | $q_e$ exp (mg $g^{-1}$) | 24.67 |
| | | $R^2$ | 0.965 |
| | PSO | $K_2$ (mg $g^{-1}$ $min^{-1}$) | 0.0050 |
| | | $q_e$ cal (mg $g^{-1}$) | 26.41 |
| | | $q_e$ exp (mg $g^{-1}$) | 24.67 |
| | | $R^2$ | 0.999 |
| | Intraparticle diffusion | $K_{int}$ (mg $g^{-1}$ min $^{-1}$/2) | 1.351 |
| | | Intercept ($C$) | 11.03 |
| | | $R^2$ | 0.772 |
| Isotherm models | Langmuir | $q_m$ (mg $g^{-1}$) | 540.3 |
| | | $b$ (L $g^{-1}$) | 0.478 |
| | | $R_L$ | 0.040 |
| | | $R^2$ | 0.9994 |
| | | $\chi^2$ | 6.94 |
| | Freundlich | $K_F$ (mg $L^{-1}$/n $g^{-1}$ $L^{-1}$) | 10.418 |
| | | $n$ | 5.216 |
| | | $R^2$ | 0.9140 |
| | | $\chi^2$ | 69.37 |

| Thermodynamic parameters | Temperature | $\Delta G$ (kJ $mol^{-1}$) | $\Delta H$ (kJ $mol^{-1}$) | $\Delta S$ (J $mol^{-1}$ $K^{-1}$) |
|---|---|---|---|---|
| | 298 K | −5.932 | 14.186 | 67.125 |
| | 313 K | −6.697 | | |
| | 323 K | −7.290 | | |
| | 333 K | −8.383 | | |

It was observed that the adsorption was favoured by rise in temperature, indicating the endothermic nature of the adsorption process (Fig. 3f). The simultaneous effect of two parameters is depicted in Fig. 3g and h. These graphs clearly indicate that a longer adsorption period, higher adsorbent dose, and lower dye concentration led to a greater percentage adsorption.

## Isotherms, kinetics, and thermodynamics of the adsorption process

Adsorption isotherms were applied as mathematical models that could be used to predict the interaction between RBBR and the Cs–C adsorbent.[46] The two isotherm models of Langmuir[47] and Freundlich[48] were applied to investigate the equilibrium isotherms of the adsorption and for calculating the $q_{max}$. The Langmuir isotherm equation in linearized form is given by:

$$\frac{C_e}{q_e} = \frac{1}{bq_m} + \frac{C_e}{q_m}$$

where $q_m$ (mg $g^{-1}$) and $b$ (L $mg^{-1}$) are Langmuir isotherm coefficients, and $q_m$ represents the maximum adsorption capacity.

$$\ln q_e = \frac{1}{n}\ln C_e + \ln K_F$$

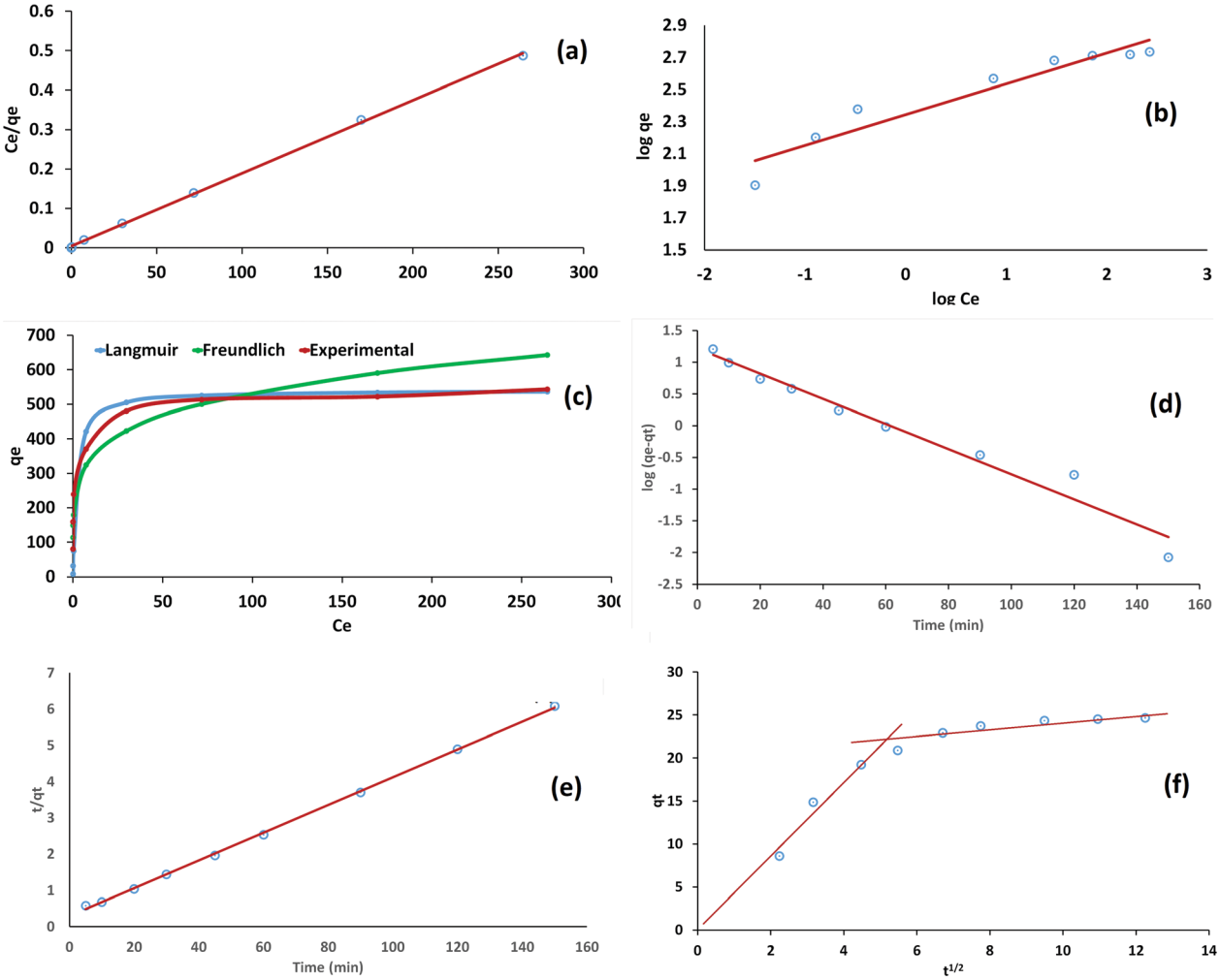


Fig. 4 (a) Langmuir, (b) Freundlich, (c) $C_e$–$q_e$ plot, (d) PFO, (e) PSO, and (f) intraparticle diffusion.

where $K_F$ and $n$ are Freundlich constants that indicate the adsorption capacity and adsorption intensity, respectively. A value of $n$ between 1 and 10 indicates favourable adsorption.

It can be clearly seen from Table 1 and Fig. 4 that the Langmuir model fitted best with the experimental data, with a coefficient of determination value very close to 1 and a smaller value of $\chi^2$, indicating monolayer adsorption on the homogeneous surface of the adsorbent. The maximum monolayer adsorption capacity obtained from the Langmuir model was found to be 540.3 mg $g^{-1}$, which showed the excellent efficiency of the material. $R_L < 1$ and $1 < n < 10$ were indications of the feasible adsorption of the dye on the Cs–C surface.

Pseudo-first-order (PFO), pseudo-second-order (PSO), and intraparticle diffusion models were applied under optimized operating conditions. The models were applied in a time-dependent study. As can be observed form Table 1 and Fig. 4, the PSO model was the best fitted model for the kinetics of adsorption. This was clear from the correlation coefficient ($R^2$) values. The calculated $q_e$ values from the PSO model were in agreement with experimental value of $q_e$, thereby suggesting that the adsorption of RBBR dye on the Cs–C surface involved chemical interactions, such as electrostatic attraction between the negative charge of RBBR dye and positive charge available on the Cs–C surface.[49] The Weber Morris intraparticle diffusion model showed that the adsorption process was diffusion controlled in the beginning with a zero intercept and linear relation between $q_t$ and $t^{1/2}$. However, with time, the process led to saturation and the boundary layer played an important role in the non-zero intercept of the graph. The overall intercept value of 11.03 indicated that the overall process was not just controlled by the diffusion.[46]

The equilibrium constant $K$ was established at different temperatures from 298 to 333 K taking the ratio of concentration of dye in the adsorbed phase to that in the solution phase. Using the equation $\Delta G^\circ = -RT\ln K$, the corresponding values of $\Delta G$ were calculated, while the values of $\Delta H$ and $\Delta S$ were calculated from the intercept and slope of the vant Hoff plot of lnK as a function of $1/T$. It was interesting to note that the adsorption process was endothermic in nature, but spontaneous over the entire temperature range and resulted in an increase in randomness. This showed the entropy-driven nature of the process (Table 1).

Table 2 Comparison of the adsorption capacities of RBBR dye by various adsorbents

| Adsorbent | $q_m$ (mg g$^{-1}$) | Ref. |
|---|---|---|
| (DTMA) bromide modified bentonite | 206.58 | 50 |
| Magnesium oxide | 250 | 51 |
| Lignocellulosic waste | 75.19 | 52 |
| Activated clay | 400 | 53 |
| Co-electrospun nanofibres | 61.2 | 54 |
| Lemna minor | 9.45 | 55 |
| Fly Ash | 47.86 | 56 |
| Metal hydroxide waste sludge | 91 | 57 |
| Mesoporous activated carbon | 35.5 | 58 |
| Fe–Al doped cellulose (FADC) | 95.62 | 59 |
| Activated charcoal from leaves of Thuja orientalis | 170 | 60 |
| Fomes fomentarius | 90 | 61 |
| Sewage sludge biochar | 126.59 | 62 |
| Yarrowia lipolytica Biomass | 103 | 63 |
| **Cs–C** | **540.3** | **Present work** |

### Probable mechanism

The activated charcoal provided the surface for the chitosan molecules to interact with the dye ions with an anionic sulphate group. Chitosan has protonated amine groups that have a strong electrostatic interaction with the anionic dye molecules. This was in accordance with the observation that increasing the pH in the basic range reduced the adsorption capacity of Cs–C and also as the $-NH_2$ peak was suppressed after adsorption of the dye molecules.

## Conclusion

A microporous crosslinked Cs–C composite was successfully synthesized and then analyzed by various characterizations. The composite was utilized to remove RBBR dye (anionic dye) from aqueous medium. Cs–C was characterized using various techniques, which confirmed the formation of a composite having STTP crosslinked well to the chitosan. SEM micrographs and EDAX analysis showed the morphological transformation and composition of Cs–C, respectively. BET surface area analysis using the nitrogen adsorption–desorption method revealed a good surface area and pore volume and also confirmed the microporous nature of the adsorbent. The amount of dye adsorption was dependent on the adsorbent dosage, temperature, and contact time. The maximum qt of Cs–C was obtained from the Langmuir model as 540.3 mg g$^{-1}$, which was quite high compared to most existing biosorbents. The thermodynamics results indicated that the adsorption process was spontaneous and endothermic in nature and was entropy driven. The adsorption mechanism of the RBBR dye on the Cs–C surface could be assigned to various types of interactions, such as electrostatic attraction, H-bonding interaction, and π–π interaction. The adsorption results indicated that Cs–C can be considered as a feasible and promising biosorbent for the removal of anionic dyes from an aqueous environment. A comparison with the reported materials, as shown in Table 2, highlights the advantage of this material over the previously reported materials for the adsorption of RBBR dye.

## Author contributions

P. N.: methodology, validation, investigation, writing first draft. D. S.: formal analysis, resources. P. B.: conceptualization, R. J.: writing: review and editing, supervision.

## Conflicts of interest

There are no conflicts to declare.

## Acknowledgements

Thanks are due to DST and UGC for funding to Department of Chemistry under various schemes. Thanks to RTM Nagpur University for URPS.

## References

1 S. Rojas and P. Horcajada, *Chem. Rev.*, 2020, **120**, 8378–8415.
2 M. Naushad, G. Sharma and Z. A. Alothman, *J. Cleaner Prod.*, 2019, **241**, 118263.
3 I. Ali, O. M. L. Alharbi, Z. A. Alothman, A. Al-Mohaimeed and A. Alwarthan, *Environ. Res.*, 2019, **170**, 389–397.
4 S. M. Wabaidur, M. Khan, M. Siddiqui, M. Otero, B. Jeon, Z. Alothman and A. Hakami, *J. Mol. Liq.*, 2020, **317**, 113916.
5 M. Khan, A. Alqadami, S. Wabaidur, M. Siddiqui, B. Jeon, S. Alshareef, Z. Alothman and A. Hamedelniel, *J. Hazard. Mater.*, 2020, **400**, 123247.
6 H. Tang, W. Zhou and L. Zhang, *J. Hazard. Mater.*, 2012, **209–210**, 218–225.
7 G. San Miguel, S. D. Lambert and N. J. D. Graham, *J. Chem. Technol. Biotechnol.*, 2006, **81**, 1685–1696.
8 Y. Al-Degs, M. A. M. Khraisheh, S. J. Allen and M. N. Ahmad, *Water Res.*, 2000, **34**, 927–935.
9 M. Beheraa, J. Nayak, S. Banerjee, S. Chakrabortty and S. K. Tripathy, *J. Environ. Chem. Eng.*, 2021, **9**, 105277.
10 A. Mittal, M. Naushad, G. Sharma, Z. A. ALothman, S. M. Wabaidur and M. Alam, *Desalin. Water Treat.*, 2016, **57**, 21863–21869.

11 A. Azhar, Y. Yamauchi, A. Allah, Z. A. Alothman, A. Badjah, M. Naushad, M. Habila, S. Wabaidur, J. Wang and M. Zakaria, *Nanomaterials*, 2019, **9**, 776.
12 A. Alqadami, M. Khan, M. Siddiqui and Z. A. Alothman, *Microporous Mesoporous Mater.*, 2018, **261**, 198–206.
13 I. Ali, O. Alharbi, Z. A. ALOthman, A. Al-Mohaimeed and A. Alwarthan, *Environ. Res.*, 2019, **170**, 389–397.
14 T. Robinson, G. McMullan, R. Marchant and P. Nigam, *Bioresour. Technol.*, 2001, **77**, 247–255.
15 Z. Li, A. Gómez-Avilés, L. Sellaoui, J. Bedia, A. Bonilla-Petriciolet and C. Belver, *Chem. Eng. J.*, 2019, **371**, 868–875.
16 A. Pala and E. Tokat, *Water Res.*, 2002, **36**, 2920–2925.
17 J. Dwyer, P. Griffiths and P. Lant, *Water Res.*, 2009, **43**, 553–561.
18 M. T. Butt, N. Imtiaz, S. Ahmed, F. Arif and S. R. Khan, *Pak. J. Sci. Ind. Res., Ser. B*, 2010, **53**, 81–84.
19 Z. Sun, Z. Sun, X. Duan, C. Srinivasakannan and J. Liang, *RSC Adv.*, 2018, **8**(16), 8625.
20 F. Yang, B. Sheng, Z. Wang, Y. Xue, J. Liu, T. Ma, R. Bush, H. Kušić and Y. Zhou, *J. Hazard. Mater.*, 2021, **406**, 124774.
21 M. D. Faysal Hossain, N. Akther and Y. Zhou, *Chin. Chem. Lett.*, 2020, **31**, 2525–2538.
22 Y. Zhou, J. Lu, Y. Zhou and Y. Liu, *Environ. Pollut.*, 2019, **252**, 352–365.
23 M. Z. Elsabee, R. E. Morsi and A. M. Al-Sabagh, *Colloids Surf., B*, 2009, **74**, 1–16.
24 M. Guo, J. Wang, C. Wang, P. J. Strong, P. Jiang, Y. S. Ok and H. Wang, *Sci. Total Environ.*, 2019, **682**, 340–347.
25 J. Yang, Y. Han, Z. Sun, X. Zhao, F. Chen, T. Wu and Y. Jiang, *ACS Omega*, 2021, **6**, 15885–15891.
26 S. Korde, S. Deshmukh, S. Tandekar and R. Jugade, *Carbohydr. Polym. Technol. Appl.*, 2021, **2**, 100081.
27 M. A. Khapre and R. M. Jugade, *Water Sci. Technol.*, 2020, **82**, 715–731.
28 S. H. Vithalkar and R. M. Jugade, *Mater. Today: Proc.*, 2020, **29**, 1025–1032.
29 M. A. Khapre, S. Pandey and R. M. Jugade, *Int. J. Biol. Macromol.*, 2021, **190**, 862–875.
30 A. H. Jawad, A. S. Abdulhameed and M. S. Mastuli, *J. Polym. Environ.*, 2020, **28**, 1095–1105.
31 E. R. Kenawy, A. A. Ghfar, S. M. Wabaidur, M. A. Khan, M. R. Siddiqui and Z. A. Alothman, *J. Environ. Manage.*, 2018, **219**, 285–293.
32 S. Kahu, A. Shekhawat, D. Saravanan and R. Jugade, *Int. J. Environ. Sci. Technol.*, 2016, **13**, 2269–2282.
33 S. Tandekar, S. Korde and R. Jugade, *Carbohydr. Polym. Technol. Appl.*, 2021, **2**, 100128.
34 D. R. Bhumkar and V. B. Pokharkar, *AAPS PharmSciTech*, 2006, **7**, E138–E143.
35 C. Theerakarunwong and D. Boontong, *Results Chem.*, 2020, **2**, 100024.
36 Z. A. Alothman, A. Bahkali, M. Khiyami, S. Alfadul, S. Wabaidur, M. Alam and B. Alfarhan, *Sep. Sci. Technol.*, 2020, **55**, 1766–1775.
37 X. Qi, L. Lin, L. Shen, Z. Li, T. Qin, Y. Qian, X. Wu, X. Wei, Q. Gong and J. Shen, *ACS Sustainable Chem. Eng.*, 2019, **7**, 11014–11023.
38 S. P. Facchi, D. B. Scariot, P. V. A. Bueno, P. R. Souza, L. C. Figueiredo, H. D. M. Follmann, C. S. Nunes, J. P. Monteiro, E. G. Bonafe, C. V. Nakamura, E. C. Muniz and A. F. Martins, *Int. J. Biol. Macromol.*, 2016, **87**, 237–245.
39 G. F. Leal, L. A. Ramos, D. H. Barrett, A. A. S. Curvelo and C. B. Rodella, *Thermochim. Acta*, 2015, **616**, 9–13.
40 S. Korde, S. Tandekar, D. Saravanan and R. Jugade, *J. Environ. Chem. Eng.*, 2020, **8**, 104360.
41 M. J. Ahmed, P. U. Okoye, E. H. Hummadi and B. H. Hameed, *Bioresour. Technol.*, 2019, **278**, 159–164.
42 S. Ahmed and A. Iqbal, *Global Challenges*, 2018, **2**, 1800056.
43 K. S. W. Sing, *Pure Appl. Chem.*, 1985, **57**, 603–619.
44 G. Ozturk and H. Silah, *Environ. Processes*, 2020, **7**, 479–492.
45 T. Khan, M. Nouman, D. Dua, S. Khan and S. Alharthi, *J. Saudi Chem. Soc.*, 2022, **26**, 101417.
46 X. Qi, M. Chen, Y. Qian, M. Liu, Z. Li, L. Shen, T. Qin, S. Zhao, Q. Zeng and J. Shen, *Int. J. Biol. Macromol.*, 2019, **132**, 429–438.
47 I. Langmuir, *J. Am. Chem. Soc.*, 1918, **40**, 1361–1403.
48 H. M. Freundlich, *Z. Phys. Chem.*, 1906, **57**, 385–470.
49 M. V. Subbaiah and D.-S. Kim, *Ecotoxicol. Environ. Saf.*, 2016, **128**, 109–117.
50 A. Ozcan, C. Omeroglu, Y. Erdogan and A. S. Ozcan, *J. Hazard. Mater.*, 2007, **140**, 173–179.
51 N. K. Nga, P. T. T. Hong, T. Dai Lam and T. Q. Huy, *J. Colloid Interface Sci.*, 2013, **398**, 210–216.
52 M. Asgher and H. N. Bhatti, *Can. J. Chem. Eng.*, 2012, **90**, 412–419.
53 R. S. Juang, F. C. Wu and R. L. Tseng, *Environ. Technol.*, 1997, **18**, 525–531.
54 R. A. Hakro, M. Mehdi, R. F. Qureshi, R. B. Mahar, M. Khatri, F. Ahmed, Z. Khatri and I. S. Kim, *Mater. Res. Express*, 2021, **8**, 055502.
55 D. Balarak, Y. Mahdavi and A. Joghataei, *Arch. Hyg. Sci.*, 2015, **4**, 199–207.
56 N. Dizge, C. Aydiner, E. Demirbas, M. Kobya and S. Kara, *J. Hazard. Mater.*, 2008, **150**, 737–746.
57 S. C. R. Santos, V. J. P. Vilar and R. A. R. Boaventura, *J. Hazard. Mater.*, 2008, **153**, 999–1008.
58 T. Silva, A. Ronix, O. Pezoti, L. Souza, P. Leandro, K. Bedin, K. Beltrame, A. Cazetta and V. Almeida, *Chem. Eng. J.*, 2016, **303**, 467–476.
59 M. Khapre, A. Shekhawat, D. Saravanan, S. Pandey and R. Jugade, *Mater. Adv.*, 2022, **3**, 3278–3285.
60 M. Arya, P. Bafila and D. Mishra, *SN Appl. Sci.*, 2020, **2**, 265.
61 C. Arslant, I. M'barek, M. Saleh, Z. Isik, S. Ozdemir, A. Dundar and N. Dizge, *Water Pract. Technol.*, 2022, **17**, 749–762.
62 A. Raj, A. Yadav, A. Rawat, A. Singh, S. Kumar, A. Pandey, R. Sirohi and A. Pandey, *Environ. Technol. Innovation*, 2021, **23**, 101556.
63 Y. D. Aracagok, *Arch. Microbiol.*, 2022, **204**, 128.